14th International Symposium on Turbulence and Shear Flow Phenomena (TSFP14)
Heidelberg, Germany, July 28–31, 2026

# SELF-SIMILAR MOTIONS OF WALL-ATTACHED STRUCTURES IN A TURBULENT BOUNDARY LAYER OVER CUBICAL ROUGHNESS

**Junwoo Jae**
School of Mechanical Engineering
Pusan National University
Busan 46241, Republic of Korea
jjw8557@pusan.ac.kr

**Min Yoon**
Department of Mechanical Engineering
Korea Maritime & Ocean University
Busan 49112, Republic of Korea
minyoon@kmou.ac.kr

**Jinyul Hwang**
School of Mechanical Engineering
Pusan National University
Busan 46241, Republic of Korea
jhwang@pusan.ac.kr

## ABSTRACT

Wall-attached structures of the streamwise velocity fluctuation ($u$) in a turbulent boundary layer (TBL) over a staggered array of cubical roughness elements with a large relative height ($k/\delta = 0.12$) are investigated using direct numerical simulation (DNS) at $Re_\tau \approx 700$. A smooth-wall TBL DNS is analysed for comparison. Wall-attached $u$ structures are identified from instantaneous flow fields and classified into $y$- and $\delta$-scaled structures according to their wall-normal height. The $y$-scaled structures are geometrically self-similar, and their two-dimensional spectra exhibit an approximately linear relationship between the streamwise and spanwise wavelengths ($\lambda_x$ and $\lambda_z$). For the $\delta$-scaled structures, the smooth wall shows limited spanwise growth for $\lambda_z > \delta$, whereas the rough wall exhibits a clearer linear trend, $\lambda_x \sim \lambda_z$. Nevertheless, energetic spectral ridges for both $y$- and $\delta$-scaled structures collapse well and align along a linear relationship over $4.5y' < \lambda_x < 3\delta$ in both cases, where $y'$ is the wall-normal distance from the virtual origin. Integration over this energetic self-similar band shows that self-similar motions dominate the logarithmic variation of the streamwise turbulence intensity and are enhanced over the rough wall. The identified structures reveal amplified meandering over the rough wall, particularly for very large and long structures. As meandering increases, the upper bound of the two-dimensional spectra approaches $\lambda_x \sim \lambda_z$, suggesting that amplified meandering redistributes energy towards larger $\lambda_z$ at long $\lambda_x$ and thereby contributes to the enhancement of self-similar motions and the logarithmic variation of the streamwise turbulence intensity.

## Introduction

The behaviour of turbulent boundary layers (TBLs) over urban- or vegetation-like rough surfaces is strongly altered by the presence of roughness obstacles (Jiménez, 2004). Over sufficiently rough walls, the viscous sublayer is effectively replaced by a roughness sublayer, and turbulence production is governed by roughness-induced shear layers and wakes rather than by the canonical smooth-wall near-wall cycle (Raupach *et al.*, 1991). Despite these pronounced near-wall modifications, whether the outer region remains similar to that over a smooth wall is still debated, particularly for surfaces composed of large three-dimensional roughness elements whose height is not negligible relative to the boundary-layer thickness (Krogstadt & Antonia, 1999; Lee *et al.*, 2011; Ahn *et al.*, 2013).

Cubical roughness has often been adopted as an idealised model of urban-like terrain. Previous studies have shown that such roughness modifies not only near-wall motions, such as low-speed streaks and quasi-streamwise vortices, but also coherent motions in the outer region (Coceal *et al.*, 2007; Lee *et al.*, 2011). In particular, the organisation and coherence of outer low-momentum regions can differ from those in smooth-wall turbulence, suggesting that the influence of cubical roughness is not confined to the near-wall region, especially when the relative roughness height is large.

A central issue in the logarithmic and outer regions concerns very large-scale motions (VLSMs) or superstructures, which carry a substantial fraction of turbulent kinetic energy and Reynolds shear stress (Kim & Adrian, 1999; Guala *et al.*, 2006; Balakumar & Adrian, 2007). These motions are known to meander strongly in the spanwise direction, which affects their apparent streamwise extent in conventional statistics (Hutchins & Marusic, 2007). Over rough walls, previous studies suggest that superstructures persist but with modified coherence and organisation. However, most of these conclusions have been drawn from statistical analyses, such as two-point correlations, POD and spectra, and less is known about how individual coherent structures are modified by roughness (Wu & Christensen, 2010).

To better understand the significance of VLSMs or superstructures in the logarithmic region, it is useful to also consider them from the perspective of Townsend's attached-eddy hypothesis (AEH), which interprets the logarithmic region in terms of hierarchies of self-similar wall-attached motions (Townsend, 1976; Perry *et al.*, 1986). Within this framework, the logarithmic variation of the streamwise turbulence intensity is regarded as a signature of self-similar energy-containing motions. VLSMs or superstructures have often been viewed as non-self-similar $\delta$-scaled motions that obscure this signature (Yoon *et al.*, 2020; Hwang *et al.*, 2020; Deshpande *et al.*, 2021). More recent studies, however, suggest a closer connection between superstructures and self-similar motions. Using high-Reynolds-number TBL data, Deshpande *et al.* (2023) showed that superstructures comprise smaller self-similar coherent motions, while Hwang & Lee (2022) showed that stronger meandering of wall-attached $u$ structures is associated with energy distributed towards larger $\lambda_z$ at long $\lambda_x$, thereby promoting a linear relationship between $\lambda_x$ and $\lambda_z$ in the logarithmic region.

These observations, together with the finding of Choi *et al.* (2020) that increasing the height of cubical roughness modifies the organisation and spanwise merging of large-scale streaky motions in the logarithmic region, motivate a direct structural investigation of TBLs over cubical roughness. In our recent DNS of a TBL over cubical roughness with a large relative roughness height ($k/\delta = 0.12$), the streamwise turbulence intensity exhibited a clear logarithmic variation even at moderate Reynolds number, whereas the corresponding smooth-wall case did not show such a clear behaviour (Yoon, 2024). The objective of the present study is therefore to examine, from a structural viewpoint, how cubical roughness modifies wall-attached $u$ structures, with particular emphasis on the meandering of very large-scale structures, and how such modifications are related to enhanced self-similar motions and the logarithmic behaviour of the streamwise turbulence intensity. To this end, we analyse DNS datasets of smooth- and rough-wall TBLs, identify wall-attached $u$ structures, and compare the self-similar motions ingrained within them.

## NUMERICAL DETAILS

In the present study, DNS datasets of zero-pressure-gradient TBLs over a smooth wall (Hwang & Sung, 2017) and over cubical roughness elements (Yoon, 2024) are analysed. The simulations were performed by solving the incompressible Navier–Stokes equations using the fractional-step method of Kim *et al.* (2002). For the rough-wall case, cubical roughness elements were represented using an immersed boundary method with discrete forcing (Kim *et al.*, 2001). More detailed descriptions of the numerical method and its validation are available in Yoon (2024).

The rough surface consists of periodically staggered cubical elements with a plan area density of $\lambda_p = 25\%$ and a large relative roughness height of $k/\delta = 0.12$, where $k$ is the cube height and $\delta$ is the boundary-layer thickness. The virtual origin $\varepsilon$ is determined following Jackson (1981), and the wall-normal distance from the virtual origin is denoted by $y' = y - \varepsilon$. For the smooth-wall case, $\varepsilon = 0$, so that $y' = y$. For the present analysis, a subdomain satisfying self-preserving conditions were extracted from the rough-wall DNS datasets. The analysed rough-wall and smooth-wall cases correspond to $Re_\tau \approx 700$ and $Re_\tau \approx 800$, respectively.

## RESULTS AND DISCUSSIONS

To analyse wall-attached structures in TBLs over cubical roughness, we identify three-dimensional clusters of the instantaneous streamwise velocity fluctuation ($u$) by extracting contiguous regions of intense $u$ (Hwang & Sung, 2018, 2019). In the three-dimensional flow field, a cluster is defined as a connected set of grid points satisfying

$$u(\mathrm{x}) > \alpha u_{\mathrm{rms}}(y') \quad \text{or} \quad u(\mathrm{x}) < -\alpha u_{\mathrm{rms}}(y'), \qquad (1)$$

where $u_{\mathrm{rms}}$ is the standard deviation of streamwise velocity and $\alpha$ is a threshold. Individual clusters are extracted using a six-neighbour connectivity rule, in which nodes are connected through their six orthogonal neighbours in Cartesian coordinates. The threshold is set to $\alpha = 1.5$ based on the percolation transition of the clusters (Hwang & Sung, 2018; Jae *et al.*, 2025).

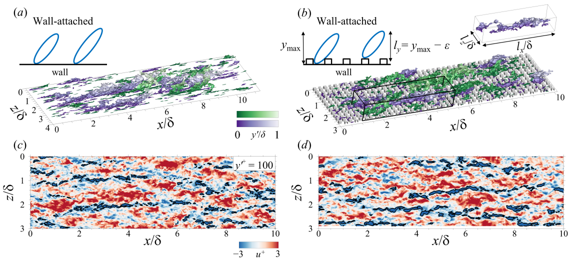

Figure 1. Identified wall-attached $u$ structures in an instantaneous flow field for the smooth-wall case (*a*) and rough-wall case (*b*). The wall-attached positive- and negative-$u$ structures are shown in green and purple, respectively, and dark shading indicates the proximity to the wall. (*c*,*d*) Contours of $u$ in the wall-parallel plane at $y'^+ = 100$ at the same instant as in (*a*,*b*). The black solid lines denote the intersection of the wall-attached negative-$u$ structures with the plane.

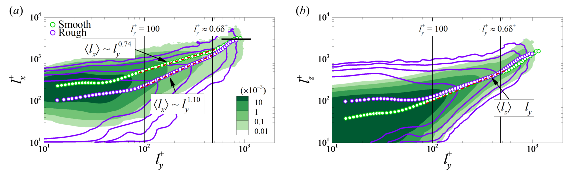

Figure 2. Contours of JPDF of the logarithms of (*a*) the streamwise length ($l_x$) and (*b*) the spanwise width ($l_z$) of wall-attached structures with respect to their wall-normal height ($l_y$). Here, coloured and line contours denote the smooth- and rough-wall cases, respectively. The inserted circle symbols indicate mean length ($\langle l_x \rangle$) and width ($\langle l_z \rangle$) at a given $l_y$, and the vertical lines represent $l_y^+ \approx 100$ and $0.6\delta^+$. In (*a*), the red dashed lines denote $\langle l_x \rangle \sim l_y^{0.74}$ and $\langle l_x \rangle \sim l_y^{1.10}$, and black horizontal line represents $\langle l_x \rangle^+ \approx 3\delta^+$. In (*b*), the red dashed line indicates $\langle l_z \rangle = l_y$.

The extracted clusters are classified as wall-attached or wall-detached according to whether they are physically anchored to the wall, following our previous study (Hwang & Sung, 2018). For the rough-wall case, structures attached to the cube surfaces are also regarded as wall-attached. Figure 1(*a*,*b*) shows instantaneous three-dimensional iso-surfaces of the wall-attached structures in the smooth- and rough-wall cases. Green and purple denote positive- and negative-$u$ structures, respectively, and the shading from light to dark indicates increasing proximity to the wall. In both cases, wall-attached structures span a wide range of wall-normal heights, from the near-wall region to the outer region.

Figure 1(*c*,*d*) shows contours of $u$ in a wall-parallel plane at $y'^+ = 100$ in the logarithmic region, taken at the same instant as in figure 1(*a*,*b*). In both cases, elongated negative-$u$ regions are observed in the streamwise direction, but the rough-wall case exhibits more pronounced spanwise meandering. The black solid lines, indicating the intersections of the wall-attached negative-$u$ structures with the plane, further show that these structures underlie the very long meandering signatures observed in the logarithmic and outer regions (Hutchins & Marusic, 2007). These observations motivate a quantitative examination of the geometrical characteristics of the wall-attached structures.

First, we examine the physical sizes of the wall-attached structures to compare their geometrical characteristics between the smooth- and rough-wall cases. The streamwise length ($l_x$) and spanwise width ($l_z$) of each structure are defined as the dimensions of its bounding box, while the wall-normal height ($l_y$) is defined as the maximum wall-normal distance from the virtual origin, i.e. $l_y = y_{\max} - \varepsilon$. For the smooth-wall case, $\varepsilon = 0$, so that $l_y = y_{\max}$. Figure 2 shows the joint probability density functions (JPDFs) of $l_x$ and $l_z$ as functions of $l_y$. In both cases, the wall-attached structures span a wide range of $l_y$, from the near-wall region to the outer region, and their wall-parallel sizes increase with increasing $l_y$. Compared with the smooth-wall case, however, the rough-wall case exhibits shorter $l_x$ over the entire range of $l_y$, implying a steeper streamwise inclination of the structures (Lee *et al.*, 2011). In addition, relatively wider structures are more prevalent in the rough-wall case at a given $l_y$.

The circles in figure 2 show the mean length ($\langle l_x \rangle$) and width ($\langle l_z \rangle$) at a given $l_y$. For $l_y^+ < 100$, clear differences are observed between the two cases, reflecting the strong influence of roughness near the wall. Over the range $100 < l_y^+ < 0.6\delta^+$, however, the two cases show good agreement in $\langle l_z \rangle$, which follows the linear relationship $\langle l_z \rangle = l_y$, consistent with previous studies (Hwang & Sung, 2018; Hwang *et al.*, 2020). In contrast, $\langle l_x \rangle$ exhibits power-law behaviours, following $\langle l_x \rangle \sim l_y^{0.74}$ for the smooth-wall case and $\langle l_x \rangle \sim l_y^{1.10}$ for the rough-wall case. Although the growth rate of $\langle l_x \rangle$ differs, both $\langle l_x \rangle$ and $\langle l_z \rangle$ scale with $l_y$ in this range, indicating that these structures are geometrically self-similar.

For $l_y^+ > 0.6\delta^+$, $\langle l_x \rangle$ deviates from this trend and, for $l_y^+ > \delta^+$, approaches a constant value of $\langle l_x \rangle^+ \approx 3\delta^+$. These very tall structures are therefore geometrically non-self-similar and can be associated with large-scale motions (LSMs) and VLSMs (Hwang *et al.*, 2020; Yoon *et al.*, 2020). Based on these scaling characteristics, we classify the wall-attached structures into three groups: buffer-layer structures for $l_y^+ < 100$, $y$-scaled structures for $100 < l_y^+ < 0.6\delta^+$, and $\delta$-scaled structures for $0.6\delta^+ < l_y^+$. Since the focus of the present study is on the logarithmic region, the following analysis concentrates on the $y$-scaled and $\delta$-scaled structures.

The previously defined length ($l_x$) and width ($l_z$) of the structures correspond to the dimensions of the bounding box of each object in physical space. In other words, these geometric measures do not necessarily reflect a characteristic length scale associated with turbulent motions ingrained within the identified structure at a given wall-parallel plane ($y' < l_y$), since the structures are inclined relative to the wall and contain a broad range of scales in the spectral domain (Hwang *et al.*, 2020). Spectral analysis is therefore required to assess whether the large scales ingrained within the classified structures exhibit spectral-overlap behaviour in the logarithmic region (Perry *et al.*, 1986), characterised by a linear relationship between $\lambda_x$ and $\lambda_z$, and whether these ingrained self-similar motions contributes to the logarithmic variation of the streamwise turbulent intensity. The pre-multiplied two-dimensional spectrum of each classified structure, $\Phi_y^{2D}$ and $\Phi_\delta^{2D}$, is defined as

$$\Phi_i^{2D}(k_x, k_z, y') = k_x k_z \left\langle \hat{u}_i(k_x, k_z, y') \hat{u}_i(k_x, k_z, y') \right\rangle, \qquad (2)$$

where the subscript $i \in \{y, \delta\}$ denotes each classified structure and $u_i$ represents the conditionally sampled $u$ within each structure. The superscript asterisk ($*$) and the hat symbol ($\hat{\cdot}$) indicate the complex conjugate and the Fourier coefficient, respectively.

Figure 3 compares the premultiplied two-dimensional spectra of the conditionally sampled streamwise velocity within the $y$- and $\delta$-scaled structures across the logarithmic region ($y'^+ = 90$, 100, and 110) for the smooth- and rough-wall cases. For the $y$-scaled structures (figure 3*a,c*), although the physical sizes of the $y$-scaled structures differ between the smooth- and rough-wall cases, the spectra show broadly similar behaviour, suggesting that the turbulent motions ingrained within them remain largely unchanged. In both cases, the constant-energy contours follow a square-root behaviour, $(\lambda_x/y')^{1/2} \sim (\lambda_z/y')$, over the intermediate range ($y' < \lambda_x < 10y'$), while in the larger-scale range ($\lambda_x > 10y'$) they approach a linear relationship, indicating the presence of self-similar energy-containing motions.

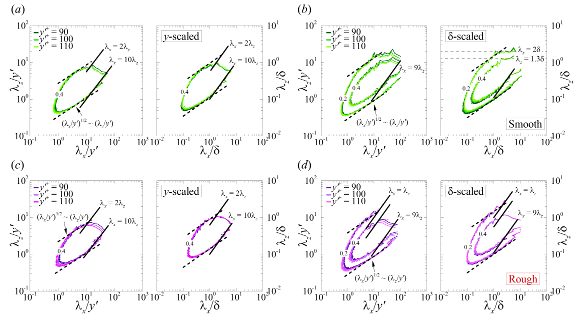


Figure 3. Premultiplied two-dimensional energy spectra across the logarithmic region ($y'^+ = 90$, 100 and 110): (*a*,*b*) smooth-wall case; (*c*,*d*) rough-wall case. Panels (*a*,*c*) show the spectra of the $y$-scaled structures, whereas panels (*b*,*d*) show those of the $\delta$-scaled structures. In each panel, the left and right subpanels show the spectra plotted in terms of the wall-parallel wavelengths ($\lambda_x, \lambda_z$) normalised by $y'$ and by $\delta$, respectively. Dark-to-light shading indicates increasing $y'$. The contour level is 0.2 and 0.4 times the local maximum at each wall-normal location. The spectra in each panel are plotted as functions of the wall-parallel wavelengths ($\lambda_x, \lambda_z$) normalised by $y'$ and by $\delta$. The dashed and solid lines denote $(\lambda_x/y')^{1/2} \sim (\lambda_z/y')$ and $\lambda_x \sim \lambda_z$, respectively.

A clearer difference appears for the $\delta$-scaled structures (figure 3*b,d*). For the smooth-wall case, the upper bound of the constant-energy contours becomes nearly horizontal in the large-scale range, indicating limited spanwise growth for $\lambda_z > \delta$. In the rough-wall case, by contrast, the upper bound follows an approximately linear relationship, $\lambda_x \sim \lambda_z$, implying that the turbulent motions within the $\delta$-scaled structures extend to larger spanwise wavelengths while retaining self-similar organisation. Nevertheless, in both cases the 40% contour lines follow the linear lower bound ($\lambda_x \sim \lambda_z$) over a narrow large-scale range of $15y' < \lambda_x < 3\delta$, suggesting that although the $\delta$-scaled structures are geometrically non-self-similar (as shown in figure 2), they can still contain self-similar energy-containing motions, albeit over a narrow range.

To further examine the self-similar motions ingrained within the $y$- and $\delta$-scaled structures, we analyse the spectral ridges of $\Phi_y^{2D}$ and $\Phi_\delta^{2D}$, following Hwang *et al.* (2020). Figure 4 shows the energetic ridges at $y'^+ = 100$ for the smooth-wall case (figure 4*a,b*) and the rough-wall case (figure 4*c,d*). Here, each ridge is defined by the value of $\lambda_z$ at which $\Phi_i^{2D}$ attains its maximum for a given $\lambda_x$, with the dark and light circles denoting the ridges of $\Phi_y^{2D}$ and $\Phi_\delta^{2D}$, respectively. In both cases, the two ridges collapse reasonably well over a wide range of scales, except in the very-large-scale range ($\lambda_x > 3\delta$). This indicates that, although the $y$- and $\delta$-scaled structures differ in their size distributions in physical space, the most energetic turbulent motions ingrained within them in the loga-

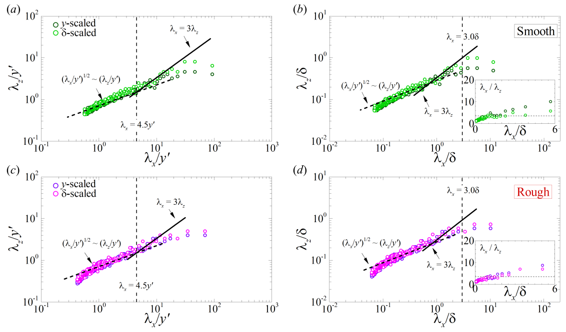


Figure 4. Energetic ridges of the pre-multiplied two-dimensional spectra at $y'^{+} = 100$: (*a,b*) smooth-wall case; (*c,d*) rough-wall case. The dark and light circles denote the spectral ridge of $\Phi_y^{2D}$ and $\Phi_\delta^{2D}$, respectively. Here, the ridge positions are obtained by identifying the value of $\lambda_z$ at which $\Phi_i^{2D}$ attains its maximum for a given $\lambda_x$. The blue dashed and solid lines represent $(\lambda_x/y')^{1/2} \sim (\lambda_z/y')$ and $\lambda_x \sim \lambda_z$, respectively. The vertical dashed lines indicate $\lambda_x = 4.5y'$ and $3\delta$. In (*b,d*), the insets show the linear–linear plot of the ridge scale ratio $\lambda_x/\lambda_z$, and the horizontal dashed line denotes a constant ratio $\lambda_x/\lambda_z \approx 3$.

rithmic region exhibit similar spectral behaviour. Moreover, despite the differences between the smooth- and rough-wall cases in figure 2, the energetic ridges remain remarkably similar, reminiscent of outer-layer similarity (Townsend, 1976). For both cases, the ridges exhibit two distinct growth regimes: a square-root relationship, $(\lambda_x/y')^{1/2} \sim (\lambda_z/y')$, and a linear relationship, $\lambda_x \sim \lambda_z$. Over the range $4.5y' < \lambda_x < 3\delta$, the linear behaviour is well approximated by $\lambda_x \approx 3\lambda_z$, as also confirmed by the nearly constant ridge ratio $\lambda_x/\lambda_z \approx 3$ shown in the insets of figure 4(*b,d*). We therefore define the range of self-similar energetic motions ingrained within the $y$- and $\delta$-scaled structures as

$$4.5y' < \lambda_x < 3\delta, \tag{3}$$

where the upper limit is comparable to the criterion commonly used to distinguish LSMs from VLSMs (Guala *et al.*, 2006; Balakumar & Adrian, 2007).

We now examine how these self-similar motions contribute to the streamwise turbulence intensity, $\langle uu\rangle^+$, by evaluating the band-average energy within this self-similar range ($4.5y' < \lambda_x < 3\delta$). The circle symbols in figure 5 show the resulting wall-normal distributions associated with the self-similar motions within each classified structure, $\langle uu\rangle^+_{y,ss}$ and $\langle uu\rangle^+_{\delta,ss}$, where green and purple denote the smooth- and rough-wall cases, respectively. For reference, the solid lines indicate the conditionally averaged streamwise turbulence intensity of the $y$-scaled structures, $\langle uu\rangle^+_y$, in figure 5(*a*) and of the $\delta$-scaled structures, $\langle uu\rangle^+_\delta$, in figure 5(*b*).

For the $y$-scaled structures (figure 5*a*), which exhibit geometrical self-similarity, $\langle uu\rangle^+_y$ follow a clear logarithmic variation in the logarithmic region for both cases, as highlighted by the dashed lines. This behaviour is consistent with previous observations that geometrically self-similar wall-attached $u$ structures give rise to a logarithmic variation in the streamwise turbulent intensity (Hwang & Sung, 2018; Hwang *et al.*, 2020). The contribution from the self-similar motions ingrained within them, $\langle uu\rangle^+_{y,ss}$, follows nearly the same logarithmic slope, indicating that the logarithmic behaviour of $\langle uu\rangle^+_y$ is predominantly supported by these self-similar motions. By contrast, for the $\delta$-scaled structures (figure 5*b*), $\langle uu\rangle^+_\delta$ does not

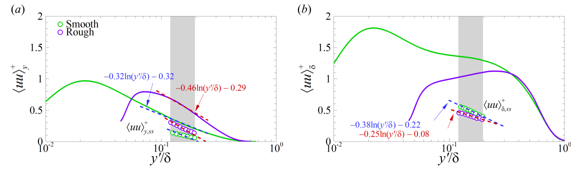


Figure 5. Wall-normal distributions of the streamwise turbulent intensity carried by each classified structure: (*a*) $\langle uu\rangle^+_y$; (*b*) $\langle uu\rangle^+_\delta$. Here, the green and purple solid lines represent the smooth- and rough-wall cases, respectively. The circles symbols indicate the streamwise turbulent intensity in the logarithmic region associated with self-similar motions ingrained within (*a*) the $y$-scaled structures, $\langle uu\rangle^+_{y,ss}$; (*b*) the $\delta$-scaled structures, $\langle uu\rangle^+_{\delta,ss}$, while the dashed lines denote logarithmic variations.

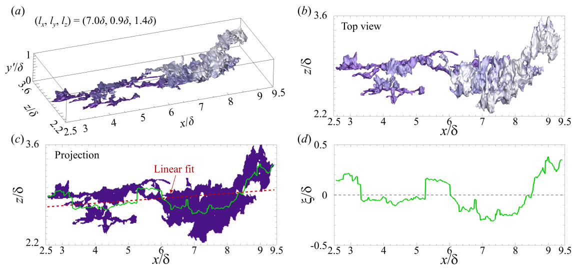


Figure 6. Instantaneous visualization of a strongly meandering wall-attached negative $u$ structure: (*a*) three-dimensional perspective view; (*b*) top view; (*c*) projection of the identified structure onto the wall (purple area), where the green line indicates the spine location ($z_{\text{spine}}$), computed as the mean spanwise position at each streamwise location; and (*d*) spanwise deviation of the spine from the linear fit ($\xi = z_{\text{spine}} - z_{\text{fit}}$). The meandering magnitude of this object is $\xi_2/\delta = 0.16$.

show a clear logarithmic variation in either case, presumably because the geometrically non-self-similar $\delta$-scaled structures also contain coexisting non-self-similar motions (Hwang *et al.*, 2020; Yoon *et al.*, 2020). However, when the contribution is restricted to the self-similar band, the resulting profiles, $\langle uu\rangle^+_{\delta,ss}$, recover a clear logarithmic variation in both cases. Moreover, although $\langle uu\rangle^+_\delta$ attains a lower level in the logarithmic region over the rough wall than over the smooth wall, the relative contribution of the ingrained self-similar motions, $\langle uu\rangle^+_{\delta,ss}/\langle uu\rangle^+_\delta$, is higher in the rough-wall case (40%) than in the smooth-wall case (35%), indicating the self-similar motions are relatively enhanced over cubical roughness.

The enhanced self-similar motions ingrained within the $\delta$-scaled structures may be related to amplified meandering of large-scale structures over cubical roughness. Hwang & Lee (2022) showed that stronger meandering allows the turbulent motions ingrained within wall-attached $u$ structures to extend to larger spanwise wavelengths while retaining a linear relationship, $\lambda_x \sim \lambda_z$. In addition, Choi *et al.* (2020) showed that increasing the height of cubical roughness elements promotes the meandering of large-scale streaks in the logarithmic region. Motivated by these observations, we now examine the enhanced self-similar motions from the perspective of the meandering of wall-attached structures.

To quantify the meandering of each identified structure, we follow the procedure of Hwang & Lee (2022). Figure 6 shows a representative large-scale streaky negative-$u$ structure and the definition of its meandering magnitude. The struc-

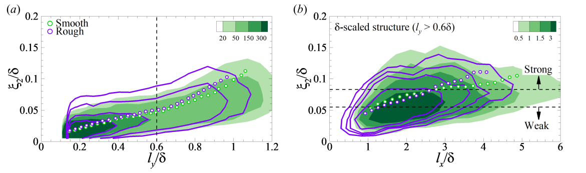


Figure 7. JPDF of meandering magnitude ($\xi_2$) of wall-attached structures. (*a*) JPDF of $\xi_2$ for structures with $l_y^+ > 100$ as a function of wall-normal height ($l_y$). (*b*) JPDF of $\xi_2$ for $\delta$-scaled structures with respect to their streamwise length ($l_x$). The coloured and line contours represent the smooth- and rough-wall cases, respectively. The circle symbols indicate mean meandering magnitude ($\langle \xi_2 \rangle$). The vertical dashed line in (*a*) denotes the $l_y/\delta = 0.6$, corresponding to the lower bound of the $\delta$-scaled structures. The horizontal dashed lines in (*b*) indicate the thresholds for the upper and lower 35% of the smooth-wall distribution.

ture is first projected onto the wall, and the spanwise spine, $z_{\mathrm{spine}}$, is defined as the midpoint between the maximum and minimum spanwise locations at each streamwise position, i.e. $z_{\mathrm{spine}} = (z_{\max} + z_{\min})/2$. A linear fit to this spine, denoted by $z_{\mathrm{fit}}$, is then obtained, and the deviation $\xi = z_{\mathrm{spine}} - z_{\mathrm{fit}}$ is taken as a measure of its waviness. The meandering magnitude, $\xi_2$, is finally defined as the root-mean-square of $\xi$ along the streamwise extent of the structure,

$$\xi_2(k) = \left( \frac{1}{l_x(k)} \int_{x_{\min}}^{x_{\max}} \xi^2(x;k), dx \right)^{1/2}, \tag{4}$$

where $x_{\min}$ and $x_{\max}$ denote the minimum and maximum streamwise locations of the $k^{\mathrm{th}}$ structure, respectively, and $l_x = x_{\max} - x_{\min}$. For the representative example in figure 6, the resulting value is $\xi_2/\delta = 0.16$, indicating substantial meandering in the streamwise direction.

Next, we explore how the meandering magnitude varies with the size of the identified wall-attached structures. Figure 7(*a*) shows the JPDF of $l_y$ and $\xi_2$, for wall-attached structures with $l_y^+ > 100$. In both cases, the structures exhibit a broad range of $\xi_2$ at a given $l_y$, and the distribution widens as $l_y$ increases. The mean meandering magnitude, $\langle \xi_2 \rangle$, shown by the circle symbols, also increases with $l_y$, indicating that taller structures tend to meander more strongly, consistent with Kevin *et al.* (2019). For the $y$-scaled structures, $\langle \xi_2 \rangle$ remains relatively small and is nearly identical in the smooth- and rough-wall cases. By contrast, the $\delta$-scaled structures exhibit substantially larger meandering magnitudes, with the rough-wall case showing consistently larger $\langle \xi_2 \rangle$ at a given $l_y$. This indicates that the meandering of very tall wall-attached structures is amplified over cubical roughness.

Figure 7(*b*) further shows the JPDF of $l_x$ and $\xi_2$ for the $\delta$-scaled structures. In both cases, $\langle \xi_2 \rangle$ increases with $l_x$, showing that longer structures tend to meander more strongly. For $l_x < 3\delta$, the two cases remain broadly similar, whereas for $l_x > 3\delta$ a clear difference emerges, with the rough-wall case exhibiting larger $\langle \xi_2 \rangle$. At the same time, the rough-wall case contains fewer extremely long structures, suggesting that cubical roughness reduces the occurrence of very long $\delta$-scaled structures while amplifying their waviness. We then further classify the $\delta$-scaled structures into three groups according to $\xi_2$: weak ($\xi_2/\delta < 0.055$), mild ($0.055 < \xi_2/\delta < 0.083$), and strong meandering ($\xi_2/\delta > 0.083$). These thresholds correspond to the lower and upper 35% quantiles of the $\xi_2$ distribution for the smooth-wall case.

To clarify how amplified meandering modifies the spectral organisation of the ingrained motions, we examine the premultiplied two-dimensional spectra of the $\delta$-scaled structures conditioned on their meandering class. Since the weak meandering structures account for only a small fraction of the total energy and exhibit spectral features similar to those of the mild class, we focus on the mild and strong meandering structures. Figure 8(*a*,*c*) shows the spectra of the strong and mild meandering structures, respectively, with the left and right subpanels denoting the smooth- and rough-wall cases. For the mild meandering structures (figure 8*c*), the constant-energy contours in both cases follow the square-root relationship, $(\lambda_x/y')^{1/2} \sim (\lambda_z/y')$, over a wide range of scales. The energetic ridges in figure 8(*d*) confirm the same tendency over nearly the entire range in both cases. By contrast, the strong meandering structures (figure 8*a*) exhibit a clear linear upper bound, $\lambda_x \sim \lambda_z$, indicating that stronger meandering is associated with turbulent motions extending to larger spanwise wavelengths while retaining self-similar organisation.

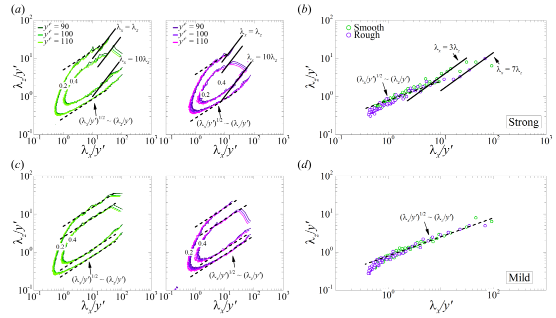


Figure 8. Premultiplied two-dimensional energy spectra of the $\delta$-scaled structures conditioned on meandering class, shown in the same format as figure 3. Panels (*a*,*b*) correspond to the strong meandering structures, and panels (*c*,*d*) to the mild meandering structures. In (*a*,*c*), the left and right subpanels denote the smooth- and rough-wall cases, respectively. Panels (*b*,*d*) show the corresponding energetic ridges at $y'^+ = 100$, where green and purple circles denote the smooth- and rough-wall cases, respectively.

The spectral ridges of the strong meandering structures, however, show a marked difference between the two cases. As shown in figure 8(*b*), the ridge in the smooth-wall case follows a linear trend close to $\lambda_x \approx 3\lambda_z$, whereas that in the rough-wall case approaches a higher-aspect-ratio relationship, $\lambda_x \approx 7\lambda_z$. Such a high-aspect-ratio linear relationship has previously been reported in the two-dimensional spectra of high-Reynolds-number TBLs by Chandran *et al.* (2017) and Deshpande *et al.* (2020). Its emergence here suggests that, even at the relatively low $Re_\tau$ of the present study, strongly meandering very long wall-attached structures, amplified by cubical roughness, can support self-similar motions with a high aspect ratio.

## CONCLUSIONS

We have investigated the contribution of self-similar motions ingrained within the wall-attached $u$ structures to the logarithmic region of a turbulent boundary layer (TBL) over cubical roughness with a large relative height ($k/\delta = 0.12$) at $Re_\tau \approx 700$, with particular emphasis on the meandering of very large-scale structures. Wall-attached $u$ structures were extracted from instantaneous flow fields and classified into $y$- and $\delta$-scaled structures according to their wall-normal height. In both smooth- and rough-wall cases, the $y$-scaled structures are geometrical self-similar and their two-dimensional spectra exhibit a linear relationship between $\lambda_x$ and $\lambda_z$, consistent with self-similarity. By contrast, the $\delta$-scaled structures, whose sizes are characterised by $\delta$, show a marked difference between the two cases: the smooth-wall case exhibits limited spanwise growth for $\lambda_z > \delta$, whereas the rough-wall case retains a clearer linear relationship, $\lambda_x \sim \lambda_z$. Despite these differences, the energetic spectral ridges of both $y$- and $\delta$-scaled structures follow $\lambda_x \approx 3\lambda_z$ in the large-scale range $4.5y' < \lambda_x < 3\delta$, indicating a range of energetic self-similar motions. Band-averaging over this range further shows that these self-similar motions dominate the logarithmic variation of the streamwise turbulence intensity and are relatively enhanced over cubical roughness. The meandering of wall-attached structures is also amplified over the rough wall, particularly for very large-scale structures. As the meandering becomes stronger, the upper bound of the two-dimensional spectra approaches $\lambda_x \sim \lambda_z$, suggesting that amplified meandering redistributes energy towards larger spanwise wavelengths at long streamwise wavelengths and thereby strengthens self-similar motions in the logarithmic region. Overall, the results indicate that amplified meandering over cubical roughness contributes to the enhancement of self-similar motions and, in turn, to the logarithmic variation of the streamwise turbulence intensity.

## ACKNOWLEDGEMENTS

This work was supported by a National Research Foundation of Korea (NRF) grant funded by the Korea government (MSIT) (No. RS-2023-00211896) and a Commercialization Promotion Agency for R&D Outcomes (COMPA) grant funded by the Korea government (MSIT) (No. RS-2023-00304764).

## REFERENCES

Ahn, Junsun, Lee, Jae Hwa & Sung, Hyung Jin 2013 Statistics of the turbulent boundary layers over 3d cube-roughened walls. *Intl J. Heat Fluid Flow* **44**, 394–402.

Balakumar, Balasubramaniam J & Adrian, Ronald J 2007 Large-and very-large-scale motions in channel and boundary-layer flows. *Phil.Trans. R. Soc. A* **365** (1852), 665–681.

Chandran, Dileep, Baidya, Rio, Monty, Jason P & Marusic, Ivan 2017 Two-dimensional energy spectra in high-Reynolds-number turbulent boundary layers. *J. Fluid Mech.* **826**, R1.

Choi, Yun Kyung, Hwang, Hyeon Gyu, Lee, Young Mo & Lee, Jae Hwa 2020 Effects of the roughness height in turbulent boundary layers over rod-and cuboid-roughened walls. *Intl J. Heat Fluid Flow* **85**, 108644.

Coceal, O, Dobre, A, Thomas, TG & Belcher, SE 2007 Structure of turbulent flow over regular arrays of cubical roughness. *J. Fluid Mech.* **589**, 375–409.

Deshpande, Rahul, Chandran, Dileep, Monty, Jason P & Marusic, Ivan 2020 Two-dimensional cross-spectrum of the streamwise velocity in turbulent boundary layers. *J. Fluid Mech.* **890**, R2.

Deshpande, Rahul, Monty, Jason P & Marusic, Ivan 2021 Active and inactive components of the streamwise velocity in wall-bounded turbulence. *J. Fluid Mech.* **914**, A5.

Deshpande, Rahul, de Silva, Charitha M & Marusic, Ivan 2023 Evidence that superstructures comprise self-similar coherent motions in high Reynolds number boundary layers. *J. Fluid Mech.* **969**, A10.

Guala, M, Hommema, SE & Adrian, RJ 2006 Large-scale and very-large-scale motions in turbulent pipe flow. *J. Fluid Mech.* **554**, 521–542.

Hutchins, Nicholas & Marusic, Ivan 2007 Evidence of very long meandering features in the logarithmic region of turbulent boundary layers. *J. Fluid Mech.* **579**, 1–28.

Hwang, Jinyul & Lee, Jae Hwa 2022 Meandering features of wall-attached structures in turbulent boundary layer. *Phys. Rev. Fluids* **7** (11), 114603.

Hwang, Jinyul, Lee, Jae Hwa & Sung, Hyung Jin 2020 Statistical behaviour of self-similar structures in canonical wall turbulence. *J. Fluid Mech.* **905**, A6.

Hwang, Jinyul & Sung, Hyung Jin 2017 Influence of large-scale motions on the frictional drag in a turbulent boundary layer. *J. Fluid Mech.* **829**, 751–779.

Hwang, Jinyul & Sung, Hyung Jin 2018 Wall-attached structures of velocity fluctuations in a turbulent boundary layer. *J. Fluid Mech.* **856**, 958–983.

Hwang, Jinyul & Sung, Hyung Jin 2019 Wall-attached clusters for the logarithmic velocity law in turbulent pipe flow. *Phys. Fluids* **31** (5).

Jackson, PS 1981 On the displacement height in the logarithmic velocity profile. *J. Fluid Mech.* **111**, 15–25.

Jae, Junwoo, Sung, Hyung Jin & Hwang, Jinyul 2025 Contribution of wall-attached momentum transfer structures to the skin friction in slip channel flows. *Intl J. Heat Fluid Flow* **112**, 109675.

Jiménez, Javier 2004 Turbulent flows over rough walls. *Annu. Rev. Fluid Mech.* **36** (1), 173–196.

Kevin, Kevin, Monty, Jason & Hutchins, Nicholas 2019 The meandering behaviour of large-scale structures in turbulent boundary layers. *J. Fluid Mech.* **865**, R1.

Kim, Jungwoo, Kim, Dongjoo & Choi, Haecheon 2001 An immersed-boundary finite-volume method for simulations of flow in complex geometries. *J. Comput. Phys.* **171** (1), 132–150.

Kim, Kyoungyoun, Baek, Seung-Jin & Sung, Hyung Jin 2002 An implicit velocity decoupling procedure for the incompressible Navier–Stokes equations. *Intl J. Numer. Meth. Fluids* **38** (2), 125–138.

Kim, Kyung Chun & Adrian, Ronald J 1999 Very large-scale motion in the outer layer. *Phys. Fluids* **11** (2), 417–422.

Krogstadt, P-Å & Antonia, RA 1999 Surface roughness effects in turbulent boundary layers. *Exp. Fluids* **27** (5), 450–460.

Lee, Jae Hwa, Sung, Hyung Jin & Krogstad, Per-Åge 2011 Direct numerical simulation of the turbulent boundary layer over a cube-roughened wall. *J. Fluid Mech.* **669**, 397–431.

Perry, AE, Henbest, S & Chong, MS0597 1986 A theoretical and experimental study of wall turbulence. *J. Fluid Mech.* **165**, 163–199.

Raupach, Michael R, Antonia, Robert Anthony & Rajagopalan, Sundara 1991 Rough-wall turbulent boundary layers. *Appl. Mech. Rev.* **4**, 1–25.

Townsend, AAR 1976 *The structure of turbulent shear flow*. Cambridge university press.

Wu, Y & Christensen, Kenneth T 2010 Spatial structure of a turbulent boundary layer with irregular surface roughness. *J. Fluid Mech.* **655**, 380–418.

Yoon, Min 2024 Direct numerical simulation of turbulent boundary layer over cubical roughness elements. *Appl. Sci.* **14** (4), 1418.

Yoon, Min, Hwang, Jinyul, Yang, Jongmin & Sung, Hyung Jin 2020 Wall-attached structures of streamwise velocity fluctuations in an adverse-pressure-gradient turbulent boundary layer. *J. Fluid Mech.* **885**, A12.